Ionics (2019) 25:1487–1494
https://doi.org/10.1007/s11581-019-02863-3

ORIGINAL PAPER

In-situ grown ultrathin MoS_2 nanosheets on MoO_2 hollow nanospheres to synthesize hierarchical nanostructures and its application in lithium-ion batteries

Jingru Xie[1] · Kunjie Zhu[1] · Jie Min[2] · Linyu Yang[3] · Jianzhe Luo[1] · Jun Liu[1] · Ming Lei[4] · Ruizhi Zhang[1] · Lu Ren[1] · Ziye Wang[5]

Received: 9 November 2018 / Revised: 22 December 2018 / Accepted: 2 January 2019 / Published online: 1 February 2019

Abstract

A unique hierarchical hollow-nanostructure consists of ultrathin MoS_2 nanosheets and hollow MoO_2 nanospheres has been designed as anode material for lithium batteries. And a simple process for producing ultrathin MoS_2 nanosheets in-situ grown on hollow MoO_2 nanospheres is reported. Such a hierarchical nanostructure has four advantages: Firstly, the high electric conductivity of the MoO_2 core can effectively increase the performance of the composite. Secondly, the shell of MoS_2 nanosheets with highly exposed active sites can improve the electrochemical reaction activity of this heterostructure. Thirdly, the reciprocal hybridization between the MoO_2 core and MoS_2 shell can availably prevent the aggregation of MoS_2 nanosheets. Owing to the unique hierarchical MoO_2@MoS_2 hollow-nanostructure, it exhibits great electrochemical performance and can deliver reversible capacity as high as 820.7 mA h g^{-1} at a current density of 0.5 A g^{-1} after 100 cycles, while it is used as a new anode material for lithium-ion batteries.

Keywords Transitional metal oxides and chalcogenides · Ultrathin MoS_2 nanosheets · Hierarchical hollow nanostructures · Lithium-ion batteries

Introduction

Rechargeable lithium-ion batteries have been applied widely in portable electronics and electric vehicles for their advantages of high energy density, high voltage, and environmental friendliness. Whereas, graphite used as commercial lithium-ion batteries, anode material has only a theoretical capacity of 372 mA h g^{-1} and cannot meet people's ever-increasing demanding of higher energy-density and power-density energy storage system [1–4]. Compared to graphite, transitional metal oxides and chalcogenides have advantages of low-cost facile fabrication and much higher specific capacity [5–9]. Among them, MoO_2 has a theoretical capacity of 838 mA h g^{-1} and high electric conductivity near to metal, but on account of internal sluggish kinetics reaction rates and accumulated volume variation in bulk MoO_2, it needs a relatively long period to activate MoO_2 and results in reversible capacity decay in a short time [10–13]. MoS_2 has a two-dimension structure like graphene with high reactivity and delivers a capacity of 800–1100 mA h g^{-1} but fades rapidly due to volume expansion and lamella staking produced in the process of charge/discharge [14–17].

To overcome the above obstacles of MoS_2 and MoO_2, many strategies have been reported. One effective strategy is to assemble MoS_2 nanosheets into the three-dimensional hierarchical structure to maintain high contact areas [18–20]. The nanosheet subunits could provide plenty of active edge sites,

Electronic supplementary material The online version of this article (https://doi.org/10.1007/s11581-019-02863-3) contains supplementary material, which is available to authorized users.

✉ Jun Liu
liujun4982004@csu.edu.cn

[1] School of Materials Science and Engineering, Central South University, Changsha 410083, Hunan, China

[2] Research Institute of Tsinghua University in Shenzhen, Shenzhen 518057, Guangdong, China

[3] School of Physics and Technology, Xin Jiang University, Urumqi, Xinjiang 830000, China

[4] State Key Laboratory of Information Photonics and Optical Communications & School of Science, Beijing University of Posts and Telecommunications, Beijing 100876, China

[5] School of Mechanical Electronic & Information Engineering, China University of Mining and Technology, Beijing 100083, China

and the primary structure could avoid the aggregation of MoS_2 nanosheets [21, 22]. Another is to synthesize MoS_2/C composite to reduce aggregation and pulverization of MoS_2 and improve its electric conductivity [23, 24].

MoO_2 has high electric conductivity and high volumetric capacity density (6.4 g cm^{-3}) compared with that of carbon. As a result, MoO_2@MoS_2 composite also has been considered as an ideal composite for Li storage. Recently, a few studies demonstrated that the MoO_2/MoS_2 composites could deliver higher specific capacity and better cycle performance compared with that of pure MoO_2 or MoS_2. Such as, Deng and co-worker synthesized ultrafine MoO_2 particles with few-layer MoS_2 delivering a high specific capacity of 787 mA h g^{-1} at 0.8 A g^{-1} [25]. Xu and co-worker fabricated MoO_2@MoS_2 nanoarchitectures by growing MoS_2 nanosheets vertically on the surface of MoO_2 particle. And its specific capacity remained 1019 mA h g^{-1} at 0.1 A g^{-1} after 200 cycles [26]. Nanocarved MoS_2-MoO_2 nanobelt hybrid was synthesized by Xiao and co-worker exhibiting impressive electrochemical performance [27]. However, the electrochemical performance of the MoO_2/MoS_2 composites in these reports has not yet gelled into a satisfying result, so additional improvement is still needed. It is highly expected that the rational design of MoO_2/MoS_2 nanostructure can effectively integrate the advantages of MoO_2 and MoS_2. Considering that, both MoO_2 and MoS_2 would have volume variation during charge/discharge process [13, 28], leading to pulverization and poor cyclability. So, the employment of hollow nanostructure would provide interior space to alleviate the strain and accommodate the volume change [29–33]. In addition, the permeable shell could also shorten the diffusion distance [19]. Therefore, synthesizing MoO_2/MoS_2 heterostructure by assembling MoS_2 subunits into three-dimensional hollow MoO_2 would be an effective way to enhance the electrochemical performance of the MoO_2/MoS_2 composites.

In this work, a unique hierarchical MoO_2@MoS_2 nanostructure consisting ultrathin MoS_2 nanosheets assembled on hollow MoO_2 nanospheres was prepared as an anode material for Li storage. Moreover, the MoO_2@MoS_2 heterostructure is synthesized via the reaction between thiourea and a solid MoO_2 nanospheres. In the reaction process, thiourea decomposes to sulfuretted hydrogen and reacts with the MoO_2 forming MoS_2 nanosheets on the surface simultaneously. Thereafter, due to the Ostwald ripening mechanism, MoO_2 core gradually dissolved and MoS_2 shell recrystallized, which finally gives rise to a hollow hierarchical MoO_2@MoS_2 nanostructure [34–36]. In this strategy, the ultrathin MoS_2 nanosheets are in-situ grown on hollow MoO_2 nanospheres. In consideration of the unique structure and the reciprocal hybridization between MoO_2 and MoS_2, it is rational to expect that MoO_2@MoS_2 heterostructure would show excellent electrochemical performance in lithium-ion batteries.

Experimental section

Material preparation

Synthesis of MoO_2: uniform MoO_2 nanospheres was firstly obtained according to our previous literature method [37]. In a typical procedure, 0.2 g MoO_3 was firstly dispersed in the mixed solution of 15 ml ethanol and 15 ml ethylene glycol, followed with stirring around 6 h. Subsequently, the milk-white solution was put into a 50-ml Teflon-lined autoclave and heated to 200 °C for 6 h. After cooling down to room temperature, the brown products were obtained by centrifugation and washed several times alternatively with distilled water and absolute ethyl alcohol then dried for 24 h at 60 °C. The dried precursors were loaded in the heating zone of quartz tube in the furnace and were calcined at 600 °C for 5 h in the atmosphere of Ar with the heating rate of 5 °C min^{-1}. After cooling down to ambient temperature, the samples were passivated in the atmosphere of 1% O_2/Ar(*v*/*v*) for 4 h.

Synthesis of MoO_2@MoS_2: the above obtained 0.16 g MoO_2 products were dispersed in 30 ml distilled water by ultrasonication for 15 min. After that, 0.32 g thiourea was added into the solution and stirred for 20 min. Then the solution was transferred into a 50-ml Teflon-lined autoclave and kept in an oven at 200 °C for 24 h. After the autoclave cooling down to ambient temperature in the oven, the black products were collected and washed with distilled water and absolute ethanol via centrifugation and dried at 60 °C for 24 h.

Material characterization

X-ray powder diffraction (XRD) to analyze the crystal structure was performed on a Rigaku D/max 2500 XRD diffractometer (Cu-Kα radiation, l 1/4 1.54178 Å). The morphology and microstructure of the products were characterized by field emission scanning electron microscope (FESEM, FEI Nova NanoSEM 230) and field emission transmission electron microscope (FETEM, Tecnai G2 F20 S-TWIN TMP). The chemical composition was evaluated by energy dispersive X-ray spectroscope (EDX). N_2 adsorption/desorption measurement was performed on Micromeritics ASPA 2460 Surface Area and Porosity Analyzer. The specific area was calculated by Brunauer-Emmett-Teller (BET) method.

Electrochemical characterization

To prepare the testing electrode, the active materials, a conductive agent (super P) and binder (polyacrylic acid) were mixed with a weight ratio of 7:2:1. Then, the mixture was dissolved in an appropriate amount of N-methyl-2-pyrrolidinone (NMP) and stirred for 24 h to obtain a homogeneous slurry. Afterward, the resulting slurry was coated on Cu foil and dried at 100 °C for 12 h under vacuum. The mass

loading of each electrode is about 1.4–1.7 mg (equals to 1.24–1.51 mg cm^{-2}). The 2016-type coin cells were then assembled in an argon-filled glove box by using lithium disc as a counter electrode, 1 M $LiPF_6$ in ethylene carbonate/dimethyl carbonate with fluoroethylene carbonate (EC/DMC, 1:1 *v*/*v* + 2%FEC) as an electrolyte, and polyethylene membrane as a separator. Galvanostatically charge/discharge (GCD) measurement was performed on a Land Battery Tester (Land CT 2001A, Wuhan, China). The cyclic voltammetry (CV) was carried on a Chi604e electrochemical workstation at a scan rate of 0.1 mV s^{-1} in the voltage range of 0.01–3 V.

Results and discussion

The crystal structure of the MoO_2@MoS_2 was characterized by XRD measurement. The pattern of MoO_2 with three major diffractions peaking at 26.2°, 36.8°, 53.7° shown in Fig. 1a could be assigned to the (-111), (-211), (-312) facet of typical monoclinic MoO_2 (JCPDS card 32-0671). It should be mentioned that the three obvious broaden peaks indicate the MoO_2 would have very small subgrain. Fig. 1b presents the XRD pattern of as-obtained MoO_2@MoS_2. It can be seen that the main three peaks were remained indicating the presence of MoO_2.

Besides, the three other pronounced peaks located at 14.4°, 32.3°, and 59.5° can be predominantly indexed to the (002), (100), and (110) planes of hexagonal 2H-MoS_2 (37-1492). The representative (002) peak of MoS_2 can also be used to calculate the interlamellar distance of the two-dimensional structure. According to the Bragg equation, the interlayer spacing is 6.2 Å. No diffraction peaks of other phase or impurities have been found proving the high-purity of the MoO_2@MoS_2.

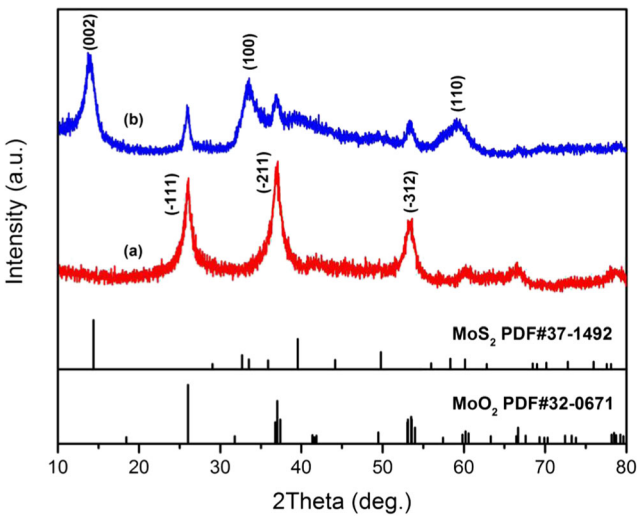

Fig. 1 XRD pattern of MoO_2 and MoO_2@MoS_2

FESEM was used to observe the morphology of the materials and the results were shown in Fig. 2.

As shown in Fig. 2a, MoO_2 has homogeneous spheres with uniform size [37]. Magnified image of MoO_2 was shown in Fig. 2b. It can be clearly observed that the surface of the spheres is relatively smooth and the size of as-formed spheres was about 500 nm. Figure 2c–d show the morphology of MoO_2@MoS_2; uniform spheres can also be found in Fig. 2c of low-magnified FESEM image. In contrast to MoO_2, it has a larger sphere size than MoO_2. Magnified FESEM image revealed that the size of MoO_2@MoS_2 is approximate 700–800 nm. Unlike the relatively smooth surface of MoO_2, MoO_2@MoS_2 has a rough surface. More specifically, the surface consists of randomly assembled ultrathin nanosheets. In our work, thiourea as the sulfur source will release sulfuretted hydrogen in the process of reaction and will react with MoO_2. The resultant is on the basis of MoO_2 spheres with MoS_2 formed and in-situ grown on MoO_2. Thus, the surface of as-formed MoO_2@MoS_2 consists of MoS_2 nanosheets and forms the hierarchical structure. Meanwhile, it can be clearly seen, there are relatively large interspaces between the MoS_2 subunits supplying extra spaces for the volume expansion in the cycling process [26]. Compared to the relatively smooth surface of as-obtained MoO_2, such secondary structure can fully utilize the two-dimension structure of MoS_2, to increase the contact areas with the electrolyte. It can boost the electrochemical reaction rates and shorten the distance, the diffusion of the ions, and electrons thus improve the electrochemical performance of the materials [38–41]. To determine the composition of MoO_2@MoS_2, EDX was carried out and the result was shown in Fig. S1. The molar ration of MoO_2 and MoS_2 is 0.31:0.69. The specific surface area was calculated by using BET method. N_2 adsorption/desorption was performed as shown in Fig. S2. The measured specific area is about 28.64 m^2 g^{-1}. Besides, it indicates a type IV curve with H3 type hysteresis. The behavior is related to the secondary capillary condensation [42, 43].

To further reveal the microstructure and morphology of the materials, TEM was applied to observe MoO_2 and MoO_2@MoS_2 and the results were shown in Fig. 3.

From the TEM image of MoO_2 in Fig. 3a, it can be observed that MoO_2 sphere is a solid structure in nature. Besides, its surface is not fully smooth and there are some small particles around the surface. In the high-resolution TEM shown in the inset of Fig. 3a, it revealed that MoO_2 is made up of small particles with the size of 20–30 nm. Such secondary structures are corresponding to the broader peaks in the XRD pattern of MoO_2. TEM image of MoO_2@MoS_2 was shown in Fig. 3b demonstrating the hollow sphere structure of as-formed MoO_2@MoS_2. Magnified images of MoO_2@MoS_2 illustrate the shell of the spheres which are composed of MoS_2 nanosheets in agreement with the SEM images, and the thickness of the shell is around 180–200 nm. High-resolution TEM

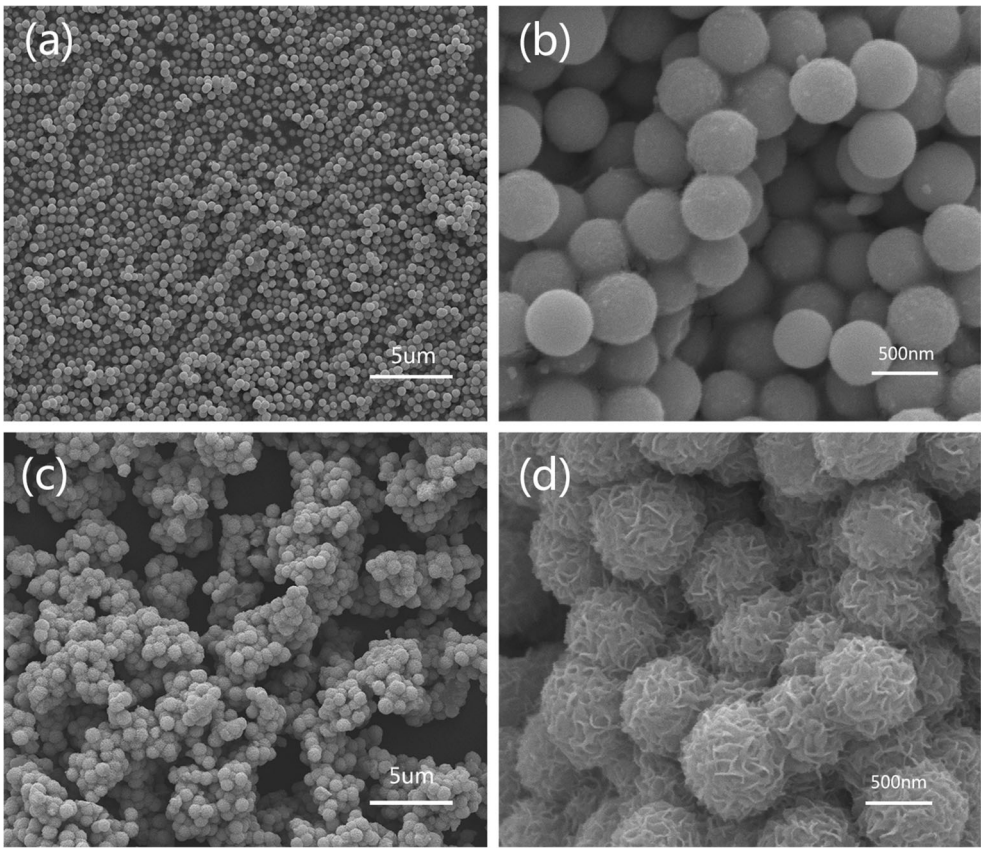

Fig. 2 FESEM images of MoO_2 spheres (**a**, **b**), and hierarchical MoO_2@MoS_2 spheres (**c**, **d**)

image shown in Fig. 3d provides further insights into the MoS_2 nanosheets of the shell. The thickness of the nanosheets is about 4–10 nm consisting of dozens of lattice planes. The lattice spacing with a distance of around 0.62 nm is consistent with the (002) facets distance value calculated from the XRD. To better understand the composition of the MoO_2@MoS_2, the scanning transmission electron microscopy and the element mapping images of MoO_2@MoS_2 are provided as shown in Fig. 3e–h. The presence of Mo, O, and S element demonstrates their uniform distribution. The intense of O is weaker because MoO_2 was in the inner shell and was coated by MoS_2. Such hollow structure could increase the contact area between electrode and electrolyte, in favor of maintaining its structure by the mean time [44, 45]. On the one side, MoO_2 in the shell can utilize the high conductivity of MoO_2 to overcome the poor conductivity of MoS_2, and the synergistic effect could also promote the reactivity of MoO_2@MoS_2 [29, 46]. On the other side, MoS_2 nanosheets with dozens of layers randomly assembled hollow sphere can improve kinetic rates of the materials and shorten the distance of ions and electrons during charging/discharging. Besides, hierarchical structure with relatively large space between nanosheets would provide extra space during charge/discharge and promote cycling stability.

To investigate the charge/discharge process of as-obtained materials, CV and GCD tests at a current density of 100 mA g^{-1} were performed as shown in Fig. 4a–b. In the first cathodic sweep, the very pronounced peak at 0.4 V can be attributed to the SEI formation and the conversion reaction of Li_xMoS_2 to Mo and Li_2S [47, 48]. It disappeared in the subsequent sweep, which indicates that it is an irreversible reaction. Except for the first discharge curve, the other curves of later charge/discharge overlap well. Strong oxidation peak at 2.25 V and reduction peak at 1.85 V are derived from the reversible reaction of Li_2S and S_8^{2-} [49, 50]. The other peaks at 1.74, 1.5, and 1.47 V are corresponding to a four-step monoclinic-orthorhombic phase transformation of Li_xMoO_2 and MoO_2 during the charge/discharge process [51, 52]. In the first discharge process shown in Fig. 4b, a potential plateau around 0.5 V corresponding to the conversion reaction in agreement with the first CV cathodic scan which indicates Li_xMoS_2 converts to Mo and Li_2S. Similar to the CV curve, other curves which overlap well indicate high reversibility except for the first discharge curve. Besides, the first discharge, specific capacity is 1122 mA h g^{-1} with the coulombic efficiency of 75% which mainly due to the irreversible reaction and formation of SEI [53, 54].

GCD under a current density of 200 mA g^{-1} was applied to investigate the electrochemical performances of materials as shown in Fig. 4c. The first discharge capacity of MoO_2@MoS_2 is 953 mA h g^{-1}, and then, the capacity fades to 902 mA h g^{-1} that lost about 5.35% which mostly originated from SEI formation and irreversible reaction. The

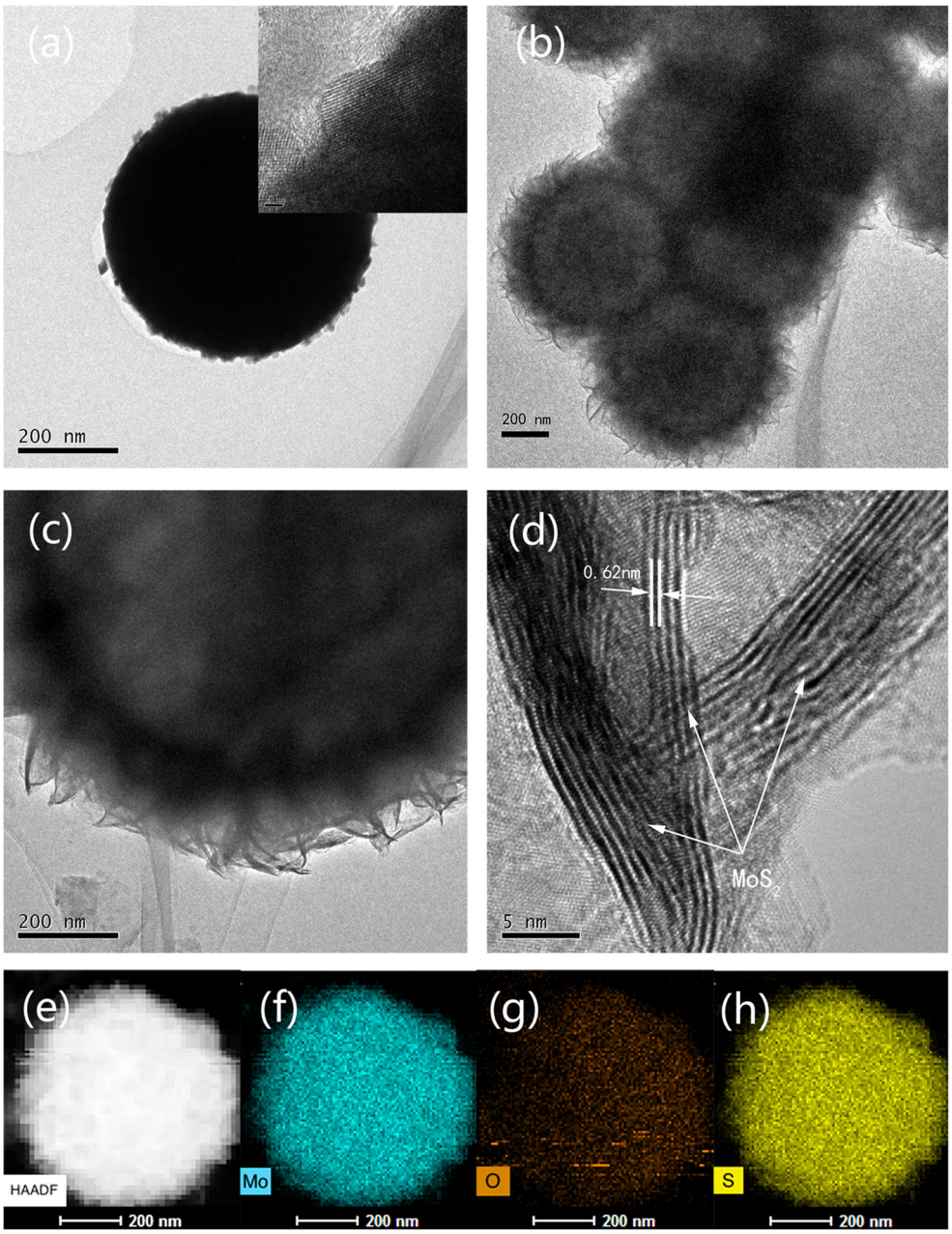

Fig. 3 TEM images of MoO_2 spheres (**a**), hierarchical MoO_2@MoS_2 spheres (**b**, **c**, **d**) and element mapping images of hierarchical MoO_2@MoS_2 (**e**–**h**)

coulomnbic efficiency in the first cycle was 85% and then maintain at around 100% showing excellent charge/discharge performances. Along with the cycling test, the capacity will slightly increase which was ascribed to the activation process of MoO_2 during the charge/discharge. It is mainly because only a certain amount of MoO_2 undergoes the conversion reaction due to the poor kinetics of Li_xMoO_2 at the beginning. But the reaction leads to partially crystallinity degradation of the MoO_2 or convert it into amorphous structures. Thus, it boosts the ion diffusion kinetics and causes more MoO_2 to undergo the reaction [55, 56]. After 50 cycles, the capacity of 917 mA h g^{-1} still can be remained with high capacity retention of 96.2% and only 3.8% decay on the basis of the first discharge capacity. In addition, rate performance is exhibited in Fig. 4d at the current density of 0.1, 0.2, 0.3, 0.5, 1.0 A g^{-1}. The first discharge capacity is 1150, 950, 890, 830, and 700 mA h g^{-1}. After current density back to 0.1 A g^{-1}, its capacity could gradually restore to about 1000 mA h g^{-1} demonstrating good capacity restore performances.

In order to compare the electrochemical performance of MoO_2 and MoO_2@MoS_2, the charge/discharge cycling test was evaluated at a current density of 500 mA g^{-1} in the voltage range of 0.01–3 V and the result is shown in Fig. 5.

The specific discharge capacity of MoO_2@MoS_2 in the first cycle was 929.7 mA h g^{-1}. A fade occurs in the second and the third cycle mainly because of the irreversible reaction. From the third cycle onwards, the capacity starts to increase due to the activation process of MoO_2. After 100 cycles, its

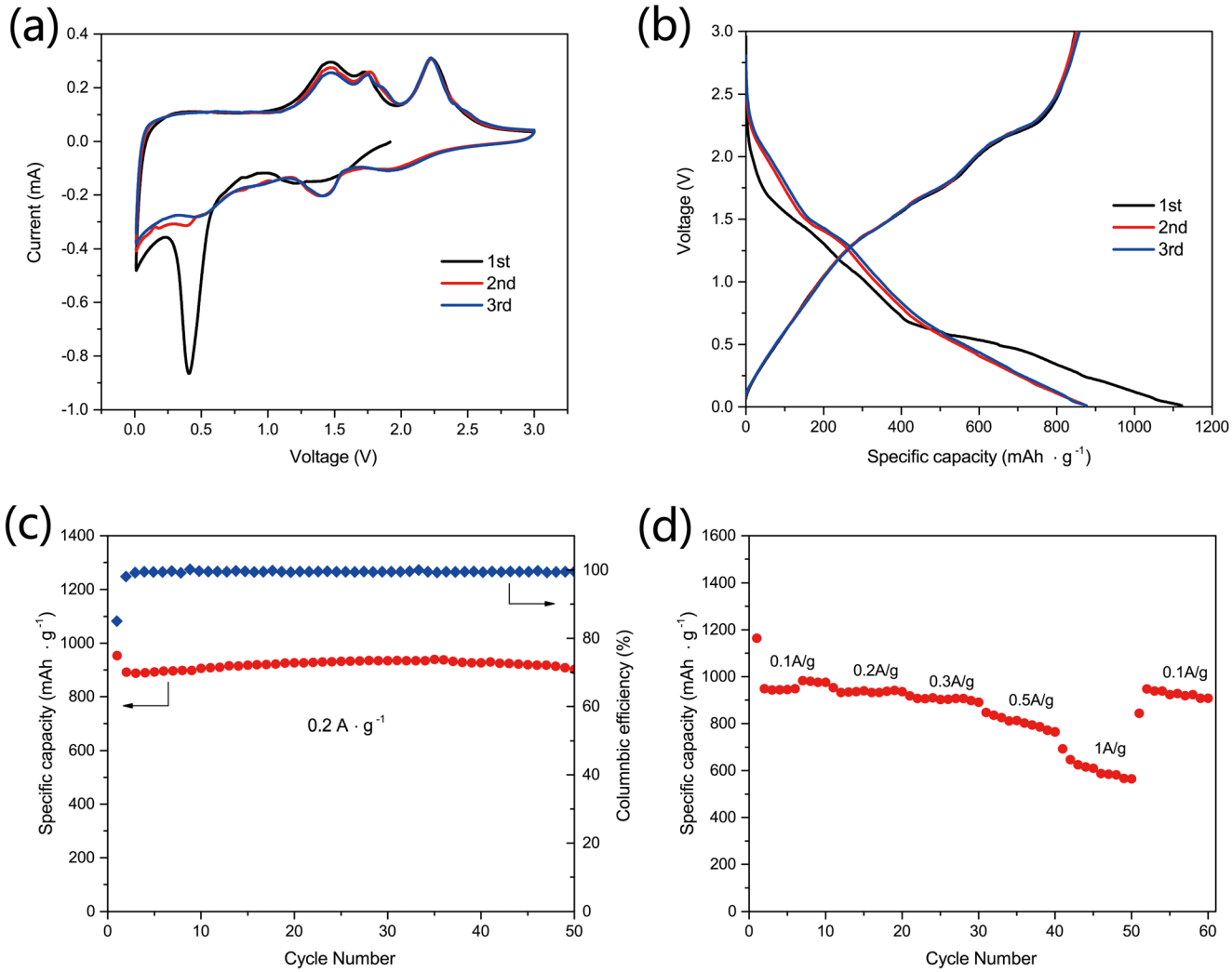

Fig. 4 **a** CV curves of first 3 cycles, **b** charge/discharge potential profile of MoO_2@MoS_2, **c** cycle performances of MoO_2@MoS_2 under a current density of 200 mA g^{-1}, and **d** rate performances of MoO_2@MoS_2

capacity still remains as 820.7 mA h g^{-1}, showing excellent cycle performance. In addition, SEM was carried out to investigate the MoO_2@MoS_2 electrode after 40 cycles as shown in Fig. S3. It can be observed that the sphere morphology could be maintained after charge/discharge process. As a contrast, the first discharge capacity of MoO_2 was 622.3 mA h g^{-1}. After that, MoO_2 underwent an activating stage, and the capacity began to rise up to the 21 cycles; the capacity reaches its peak of 752.7 mA h g^{-1}. After 100 cycles, the capacity of MoO_2 faded to 557.3 mA h g^{-1}. In contrast to MoO_2, MoO_2@MoS_2 delivers higher capacity accompanying with less fade and displayed better cycling stability and energy storage performance.

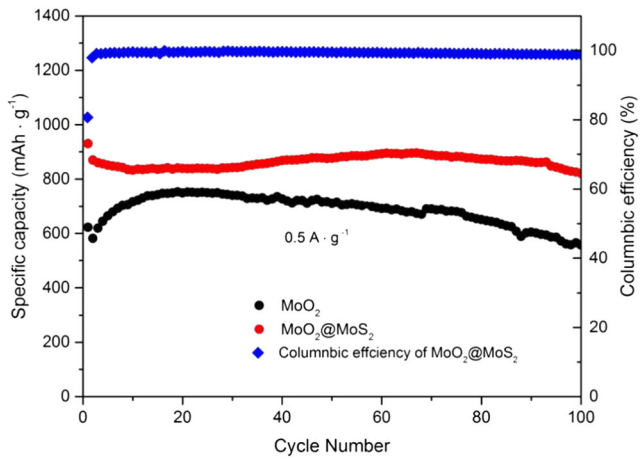

Fig. 5 Cycle performances of MoO_2 and MoO_2@MoS_2 at the current density of 0.5 A g^{-1}

Conclusions

In summary, we successfully synthesized hierarchical MoO_2@MoS_2 hollow-nanostructure consisting of ultrathin MoS_2 nanosheets and a hollow MoO_2 nanospheres. This strategy only involves a facile method via thiourea reaction with

uniform solid MoO_2 nanospheres, which leads ultrathin MoS_2 nanosheets in-situ grown on hollow MoO_2 nanospheres. The obtained hierarchical MoO_2@MoS_2 hollow-nanostructure integrated the advantages of the high conductivity of MoO_2 and the two-dimensional structure of MoS_2 to improve the electrochemical reaction activity. When evaluated as anode materials of lithium batteries, it delivers the specific capacity of 1150 mA h g^{-1} in the first cycle at the current density of 100 mA g^{-1} and still remains the specific capacity of 820.7 mA h g^{-1} after charge/discharge for 100 cycles at a current density of 500 mA g^{-1}. Compared to MoO_2, it exhibits better energy storage performances owing to the advantages of unique secondary hierarchical hollow structures.

Funding information This work is supported by the National Natural Science Foundation of China (Grant Nos. 51772331, 51472271), the National Basic Research Program of China (973 Program) grant No. 2013CB932901, and the Project of Innovation-driven Plan in Central South University (2016CX002).

References

1. Zhao C, Kong J, Yao X, Tang X, Dong Y, Phua SL, Lu X (2014) Thin MoS_2 nanoflakes encapsulated in carbon nanofibers as high-performance anodes for lithium-ion batteries. ACS Appl Mater Interfaces 6:6392–6398
2. Li HZ, Yang LY, Liu J, Li ST, Fang LB, Lu YK, Yang HR, Liu SL, Lei M (2016) Improved electrochemical performance of yolk-shell structured SnO_2@void@C porous nanowires as anode for lithium and sodium batteries. J Power Sources 324:780–787
3. Pan X, Li S, Wang Z, Yang L-Y, Zhu K, Ren L, Lei M, Liu J (2017) Core–shell MoO_2/C nanospheres embedded in bubble sheet-like carbon film as lithium ion battery anodes. Mater Lett 199:139–142
4. Lu Y, Wu J, Liu J, Lei M, Tang S, Lu P, Yang L, Yang H, Yang Q (2015) Facile synthesis of $Na_{0.33}V_2O_5$ nanosheet-graphene hybrids as ultrahigh performance cathode materials for lithium ion batteries. ACS Appl Mater Interfaces 7:17433–17440
5. Zhou J, Qin J, Zhang X, Shi C, Liu E, Li J, Zhao N, He C (2015) 2D space-confined synthesis of few-layer MoS2 anchored on carbon nanosheet for lithium-ion battery anode. ACS Nano 9:3837–3848
6. Tan C, Zhang H (2015) Two-dimensional transition metal dichalcogenide nanosheet-based composites. Chem Soc Rev 44: 2713–2731
7. Zhong W, Tu W, Feng S, Xu A (2019) Photocatalytic H2 evolution on CdS nanoparticles by loading FeSe nanorods as co-catalyst under visible light irradiation. J Alloy Compounds 772:669–674
8. Huang X, Zeng Z, Zhang H (2013) Metal dichalcogenide nanosheets: preparation, properties and applications. Chem Soc Rev 42:1934–1946
9. Huang X, Cai X, Xu D, Chen W, Wang S, Zhou W, Meng Y, Fang Y, Yu X (2018) Hierarchical Fe_2- O_3@CNF fabric decorated with MoS_2 nanosheets as a robust anode for flexible lithium-ion batteries exhibiting ultrahigh areal capacity. J Mater Chem A 6:16890–16899
10. Wang Z, Chen JS, Zhu T, Madhavi S, Lou XW (2010) One-pot synthesis of uniform carbon-coated MoO_2 nanospheres for high-rate reversible lithium storage. Chem Commun 46:6906–6908
11. Petnikota S, Teo KW, Chen L, Sim A, Marka SK, Reddy MV, Srikanth VV, Adams S, Chowdari BV (2016) Exfoliated graphene oxide/MoO_2 composites as anode materials in lithium-ion batteries: an insight into intercalation of Li and conversion mechanism of MoO_2. ACS Appl Mater Interfaces 8:10884–10896
12. Zhang P, Zou L, Hu H, Wang M, Fang J, Lai Y, Li J (2017) 3D hierarchical carbon microflowers decorated with MoO_2 nanoparticles for lithium ion batteries. Electrochim Acta 250:219–227
13. Wang S, Zhang Z, Yang Y, Tang Z (2017) Efficient lithium-ion storage by hierarchical core-shell TiO_2 nanowires decorated with MoO_2 quantum dots encapsulated in carbon nanosheets. ACS Appl Mater Interfaces 9:23741–23747
14. Yu XY, Yu L, Lou XW (2016) Metal sulfide hollow nanostructures for electrochemical energy storage. Adv Energy Mater 6:1501333
15. Nguyen QH, Hur J (2019) MoS_2–TiC–C nanocomposites as new anode materials for high-performance lithium-ion batteries. J Nanosci Nanotechnol 19:996–1000
16. Li X, Zai J, Xiang S, Liu Y, He X, Xu Z, Wang K, Ma Z, Qian X (2016) Regeneration of metal sulfides in the delithiation process: the key to cyclic stability. Adv Energy Mater 6:1601056
17. Jiang H, Ren D, Wang H, Hu Y, Guo S, Yuan H, Hu P, Zhang L, Li C (2015) 2D monolayer MoS_2-carbon interoverlapped superstructure: engineering ideal atomic interface for lithium ion storage. Adv Mater 27:3687–3695
18. Wang PP, Sun H, Ji Y, Li W, Wang X (2014) Three-dimensional assembly of single-layered MoS_2. Adv Mater 26:964–969
19. Wang M, Li G, Xu H, Qian Y, Yang J (2013) Enhanced lithium storage performances of hierarchical hollow MoS2 nanoparticles assembled from nanosheets. ACS Appl Mater Interfaces 5:1003–1008
20. Wang Y, Yu L, Lou XW (2016) Synthesis of highly uniform molybdenum–glycerate spheres and their conversion into hierarchical MoS2 hollow nanospheres for lithium-ion batteries. Angew Chem Int Ed 55:7423–7426
21. Zhang L, Wu HB, Yan Y, Wang X, Lou XW (2014) Hierarchical MoS_2 microboxes constructed by nanosheets with enhanced electrochemical properties for lithium storage and water splitting. Energy Environ Sci 7:3302–3306
22. Yan Y, Ge X, Liu Z, Wang JY, Lee JM, Wang X (2013) Facile synthesis of low crystalline MoS_2 nanosheet-coated CNTs for enhanced hydrogen evolution reaction. Nanoscale 5:7768–7771
23. Zhu C, Mu X, van Aken PA, Yu Y, Maier J (2014) Single-layered ultrasmall nanoplates of MoS_2 embedded in carbon nanofibers with excellent electrochemical performance for lithium and sodium storage. Angew Chem Int Ed 53:2152–2156
24. Chen YM, Yu XY, Li Z, Paik U, Lou XW (2016) Hierarchical MoS2 tubular structures internally wired by carbon nanotubes as a highly stable anode material for lithium-ion batteries. Sci Adv 2: e1600021
25. Deng Z, Hu Y, Ren D, Lin S, Jiang H, Li C (2015) Reciprocal hybridization of MoO_2 nanoparticles and few-layer MoS_2 for stable lithium-ion batteries. Chem Commun 51:13838–13841
26. Xu Z, Wang T, Kong L, Yao K, Fu H, Li K, Cao L, Huang J, Zhang Q (2017) MoO_2@MoS_2 Nanoarchitectures for high-loading advanced lithium-ion battery anodes. Part Part Syst Charact 34: 1600223
27. Xiao D, Zhang J, Li X, Zhao D, Huang H, Huang J, Cao D, Li Z, Niu C (2016) Nano-carved MoS_2-MoO_2 hybrids fabricated using in situ grown MoS_2 as nano-masks. ACS Nano 10:9509–9515
28. Chen B, Liu E, Cao T, He F, Shi C, He C, Ma L, Li Q, Li J, Zhao N (2017) Controllable graphene incorporation and defect engineering in MoS_2-TiO_2 based composites: towards high-performance lithium-ion batteries anode materials. Nano Energy 33:247–256
29. Zhang L, Lou XW (2014) Hierarchical MoS_2 shells supported on carbon spheres for highly reversible lithium storage. Chem Eur J 20:5219–5223

30. Zhang G, Xia BY, Xiao C, Yu L, Wang X, Xie Y, Lou XW (2013) General formation of complex tubular nanostructures of metal oxides for the oxygen reduction reaction and lithium-ion batteries. Angew Chem Int Ed 125:8916–8916
31. Yu L, Zhang L, Wu HB, Lou XW (2014) Formation of $Ni_xCo_{3-x}S_4$ hollow nanoprisms with enhanced pseudocapacitive properties. Angew Chem Int Ed 53:3711–3714
32. Wang S, Guan BY, Yu L, Lou XW (2017) Rational design of three-layered TiO_2@ carbon@ MoS_2 hierarchical nanotubes for enhanced lithium storage. Adv Mater 29:1702724
33. Lu J, Xia G, Gong S, Wang C, Jiang P, Lin Z, Wang D, Yang Y, Chen Q (2018) Metallic 1T phase MoS_2 nanosheets decorated hollow cobalt sulfide polyhedrons for high-performance lithium storage. J Mater Chem A 6:12613–12622
34. Li P, Jeong JY, Jin B, Zhang K, Park JH (2018) Vertically oriented MoS_2 with spatially controlled geometry on nitrogenous graphene sheets for high-performance sodium-ion batteries. Adv Energy Mater 8:1703300
35. Zhang Y, Wang C, Hou H, Zou G, Ji X (2017) Nitrogen doped/carbon tuning yolk-like TiO_2 and its remarkable impact on sodium storage performances. Adv Energy Mater 7:1600173
36. Weng W, Lin J, Du Y, Ge X, Zhou X, Bao J (2018) Template-free synthesis of metal oxide hollow micro-/nanospheres via Ostwald ripening for lithium-ion batteries. J Mater Chem A 6:10168–10175
37. Min J, Wang K, Liu J, Yao Y, Wang W, Yang L, Zhang R, Lei M (2017) Facile synthesis of uniform MoO_2/Mo_2CT_x heteromicrospheres as high-performance anode materials for lithium-ion batteries. J Power Sources 363:392–403
38. Wang Y, Ma Z, Chen Y, Zou M, Yousaf M, Yang Y, Yang L, Cao A, Han RPS (2016) Controlled synthesis of core-shell carbon@MoS_2 nanotube sponges as high-performance battery electrodes. Adv Mater 28:10175–10181
39. Teng Y, Zhao H, Zhang Z, Li Z, Xia Q, Zhang Y, Zhao L, Du X, Du Z, Lv P, Świerczek K (2016) MoS_2 nanosheets vertically grown on graphene sheets for lithium-ion battery anodes. ACS Nano 10: 8526–8535
40. Chang K, Chen W (2011) L-cysteine-assisted synthesis of layered MoS_2 graphene composites with excellent electrochemical performances for lithium ion batteries. ACS Nano 5:4720–4728
41. Jing Y, Ortiz-Quiles EO, Cabrera CR, Chen Z, Zhou Z (2014) Layer-by-layer hybrids of MoS_2 and reduced graphene oxide for lithium ion batteries. Electrochim Acta 147:392–400
42. Sing KS, Williams RT (2004) Physisorption hysteresis loops and the characterization of nanoporous materials. Adsorpt Sci Technol 22:773–782
43. Xie T, Min J, Liu J, Chen J, Fu D, Zhang R, Zhu K, Lei M (2018) Synthesis of mesoporous Co_3O_4 nanosheet-assembled hollow spheres towards efficient electrocatalytic oxygen evolution. J Alloys Compounds 754:72–77
44. Chang K, Geng D, Li X, Yang J, Tang Y, Cai M, Li R, Sun X (2013) Ultrathin MoS_2/nitrogen-doped graphene nanosheets with highly reversible lithium storage. Adv Energy Mater 3:839–844
45. Zhong W, Shen S, Feng S, Lin Z, Wang Z, Fang B (2018) Facile fabrication of alveolate $Cu_{2-x}Se$ microsheets as a new visible-light photocatalyst for discoloration of Rhodamine B. CrystEngComm 20:7851–7856
46. Chen B, Liu E, He F, Shi C, He C, Li J, Zhao N (2016) 2D sandwich-like carbon-coated ultrathin TiO_2-@defect-rich MoS_2 hybrid nanosheets: synergistic-effect-promoted electrochemical performance for lithium ion batteries. Nano Energy 26:541–549
47. Jeong JM, Lee KG, Chang SJ, Kim JW, Han YK, Lee SJ, Choi BG (2015) Ultrathin sandwich-like MoS_2@N-doped carbon nanosheets for anodes of lithium ion batteries. Nanoscale 7:324–329
48. Hu L, Ren Y, Yang H, Xu Q (2014) Fabrication of 3D hierarchical MoS_2/polyaniline and MoS_2/C architectures for lithium-ion battery applications. ACS Appl Mater Interfaces 6:14644–14652
49. Kong D, He H, Song Q, Wang B, Lv W, Yang Q-H, Zhi L (2014) Rational design of MoS_2@graphene nanocables: towards high performance electrode materials for lithium ion batteries. Energy Environ Sci 7:3320–3325
50. Fang X, Hua C, Guo X, Hu Y, Wang Z, Gao X, Wu F, Wang J, Chen L (2012) Lithium storage in commercial MoS_2 in different potential ranges. Electrochim Acta 81:155–160
51. Liu J, Tang S, Lu Y, Cai G, Liang S, Wang W, Chen X (2013) Synthesis of Mo_2N nanolayer coated MoO_2 hollow nanostructures as high-performance anode materials for lithium-ion batteries. Energy Environ Sci 6:2691–2697
52. Yang Q, Liang Q, Liu J, Liang S, Tang S, Lu P, Lu Y (2014) Ultrafine MoO_2 nanoparticles grown on graphene sheets as anode materials for lithium-ion batteries. Mater Lett 127:32–35
53. Ma L, Huang G, Chen W, Wang Z, Ye J, Li H, Chen D, Lee JY (2014) Cationic surfactant-assisted hydrothermal synthesis of few-layer molybdenum disulfide/graphene composites: microstructure and electrochemical lithium storage. J Power Sources 264:262–271
54. Choi SH, Kang YC (2015) Synergetic effect of yolk-shell structure and uniform mixing of SnS-MoS_2 nanocrystals for improved Na-ion storage capabilities. ACS Appl Mater Interfaces 7:24694–24702
55. Guo B, Fang X, Li B, Shi Y, Ouyang C, Hu YS, Wang Z, Stucky GD, Chen L (2012) Synthesis and lithium storage mechanism of ultrafine MoO_2 nanorods. Chem Mater 24:457–463
56. Reddy MV, Rao GVS, Chowdari BVR (2013) Metal oxides and oxysalts as anode materials for Li ion batteries. Chem Rev 113: 5364–5457